Effect of weld parameters on joint quality in friction stir welding of Mg alloy to DP steel dissimilar materials

Suryakanta Sahu[1], Omkar Mypati[2], Surjya K Pal[2*], Mahadev Shome[3], Prakash Srirangam[4]

[1]Advanced Technology Development Centre, Indian Institute of Technology Kharagpur, Kharagpur, West Bengal, 721302, India

[2] Friction Stir Welding Laboratory, Department of Mechanical Engineering, Indian Institute of Technology Kharagpur, Kharagpur, West Bengal, 721302, India

[3] Materials Welding and Joining, Research and Development, Tata Steel, Jharkhand, 831001, India

[4] Warwick Manufacturing Group, University of Warwick, Coventry, CV4 7AL, United Kingdom

Abstract

Dissimilar material joining between magnesium (AZ31B) alloy and dual-phase steel (DP600) was achieved using the friction stir welding (FSW) process. The present work aimed at studying the effect of tool rotational speed and welding speed on the microstructure and mechanical properties of the dissimilar joints. The joints were fabricated at tool rotational speeds of 800 and 1600 rpm with weld speeds of 50, 100, and 150 mm/minute, respectively. The plunge depth of 0.2 mm and tool tilt angle of 2^o was kept constant during the welding. Temperature rise and variation of torque during the welding process were recorded. Optical microscopy, scanning electron microscopy equipped with energy dispersive spectroscopy (EDS), and X-ray diffraction studies were carried out to understand the microstructural changes, the interface of the weld joints, fracture morphology, and formation of intermetallic compounds during FSW. Maximum joint efficiency of 76.4% was achieved with respect to AZ31B. The microstructural observation revealed the formation of finer grains at the stir zone for all weld parameters because of the dynamic recrystallization. The metallurgical bonding between the dissimilar materials was observed due to the formation of intermetallic compounds. The formation of the sawtooth profile at the joint interface indicated mechanical interlocking between AZ31B Mg alloy and DP600 steel. Though the AZ31B Mg-DP600 steel combination is highly immiscible, the present attempts have successfully created the joining, where one of the substrates provides lightweight while the other provides strength.

Keywords: Friction stir welding, Lap joint, Dissimilar joining, AZ31B Mg alloy, DP600 steel

Introduction

Recently, there has been a tremendous increase in demand for multi-material components in the automotive sector to manufacture lighter-weight vehicles with enhanced fuel efficiency and better collision safety [1]. To achieve these requirements, a proper selection of lightweight materials and an appropriate joining methodology for these materials are of significant concern in the research community. Presently, magnesium (Mg) and aluminium (Al) alloys are being widely used in the automotive industries as light materials compared to their counterparts, and hence can result in increased fuel efficiency [2]. Further, the use of Mg alloys over Al alloys has increased substantially because of their lower density, higher specific strength, rigidity, higher heat, and electrical conductivity [3]. Among different Mg alloys, AZ31B alloy (consisting of 3.0 wt. % of Al and 1.0 wt. % of Zn) has been used extensively owing to its excellent weldability characteristics [4]. Mg and its alloys are currently used in engines, steering column, steering wheel core, car seat frame, instrument panel, lift gate, transfer case, and door inner panels. For the vehicles, apart from being lightweight and fuel-efficient, they also need to sustain high-impact energy during the event of a crash without compromising passenger safety. Hence, instead of conventional steels, dual-phase (DP) steels like DP600 are being employed in automotive manufacturing for achieving a more excellent combination of strength and ductility, thus, absorption of high impact energy during crash [5]. DP600 steel is used for floor panel, hood outer, body side outer, and floor reinforcements. Therefore, to combine AZ31B Mg alloy and DP 600 steel properties, a suitable welding technique needs to be developed.

Dissimilar welding can be done either by using fusion welding or solid-state welding techniques. In the past, various fusion welding methods, such as resistance spot welding, laser beam welding, and laser-tungsten inert gas hybrid welding, have been applied for the same. However, due to the significant differences in the melting temperatures of the dissimilar materials, the technique possesses several challenges [6]. Furthermore, several other glitches like the distortion in plates, solidification cracking, wide heat affected zone (HAZ), and high residual stresses developed during the fusion welding process limiting its application for joining the above two dissimilar materials. Also, the immiscible characteristic of Mg/Fe in both solid and liquid states possesses an additional hindrance during welding the two materials [7]. Hence, considering the loopholes in the fusion welding processes, the solid-state joining method such as friction stir welding (FSW) can be proven to be a better alternative for the fusion welding process [8]. The FSW process is one of the robust solutions for the welding of two different material combinations. A rotating tool is used for FSW with

features, namely shoulder, and a pin, which plunges at the joint line of the substrates, and moves along the same to complete the joining process. Welding parameters such as welding speed (v), tilt angle (α), tool rotational speed (ω), and plunge depth (pd) control the joint characteristics, and a suitable combination of these parameters provides sound joint. Generally, this type of welding process occurs below the melting temperature of the individual metals, reducing the defects associated with fusion welding processes.

In recent years, several studies on dissimilar metals joining by the FSW technique have been conducted. The industrial acceptance of this technique has already been found in several applications [9]. One of the significant automobile applications is joining a dissimilar combination of Al to steel in lap configuration for the front sub-frame of Honda Accord 2013 [10]. It provides better mechanical and metallurgical properties. The material bonding across the joint interface occurs due to mechanical/metallurgical phenomena, both driven by heat and deformation [11]. While metallurgical bonding leads to different IMCs, interlocking refers to mating the base materials at the joint interface. However, only mechanical bonding has been reported in Mg/Fe, which is probably due to the immiscible characteristics of these materials at the solid and liquid states [7].

The research for joining Mg to steel by FSW can generally be categorized into two general directions: (a) parametric studies, including the variation in ω, v, and tool pin length, and (b) evaluating the dissimilar metals bonding. The influence of pin length on mechanical and microstructural properties of welded AZ31B (Mg alloy) and low carbon steel was investigated. The bonding was achieved due to the diffusion of Mg in the steel substrate. Higher pin length was found to increase the fracture load in bare steel, whereas the failure load decreased due to void formation at the joint interface [6]. Though the pin length was varied, the study only considered one combination of ω and v; thus, it limited the reported investigations. This forms an open area where further research is required.

Further, parametric study such as the effect of varying v keeping ω constant has been evaluated for alloys of Mg and Zn coated steel [12]. With increasing v, the failure load decreased due to a decrease in heat input. This essentially reduced the stirring effect between the base materials and resulted in a joint efficiency of 65% compared with Zn coated steel. The variation of v on temperature profile and mechanical properties keeping ω constant has been analyzed for AZ31 and ultra-low carbon steel joints in lap configuration. The failure strength of Zn coated samples was higher, and it increased with the rise in v [13].

Similarly, the effect of tool design and v on mechanical and microstructural properties during the joining of AZ31B and SUS302 steel was investigated. Effects such as the *"nail effect"* known by extended flash and *"zipper effect"* by sawtooth were the reasons for higher strength at higher values of v [14]. Although the interface characteristics and joint strength were investigated, the metallurgical bonding phenomenon regarding IMCs generation at the interface has not been examined. In another work, researchers have achieved a higher fracture load during the joining of AZ31B, and Zn coated steel sheets, which suffices the benefit of Zn over the steel substrate [15]. Chen and Nakata [12,15] have mainly evaluated the coating, and there is no mention of the coating thickness and its role during joining.

Furthermore, in the study of Chen and Nakata [12], the effect of ω could have been studied to see the effect of heat generation on weld quality. The feasibility of joining AZ31 with two different automotive-grade steel-grade sheets, i.e., the first being high strength low alloy and the second being electro-galvanized. The hook-like feature, which was present at the interface joint, introduced stress concentration leading to lower failure loads [7]. This article mentioned the utility of force measurement with respect to hook formation, but the effect of temperature on the microstructure and microhardness is missing.

Growing by the current trend towards the light-weighting of structures, the combination of AZ31B Mg alloy-DP600 steel has been considered in the present investigation. Attempts have been made to perform the following: (a) a parametric study considering the influence of ω and v on the mechanical properties and metallurgical bonding (IMCs), and (b) analysis of weld performance due to the aforementioned mechanical and metallurgical aspects.

2 Experimental details

2.1 Welding method

The FSW process is one of the potential solutions for the welding of two different material combinations. A rotating tool is used for FSW with features, namely shoulder, and a pin, which plunges at the joint line of the substrates, and moves along the same to complete the joining process. Welding parameters such as tool rotational speed (ω), welding speed (v), tilt angle (α), and plunge depth (pd) control the joint characteristics, and a suitable combination of these parameters provides sound joint. Parameters ω, and v, are responsible for the heat generation for joining. Also, the parametric combination of ω and v is an essential aspect of the joint quality. Besides this, a suitable α is provided, which helps in plunging and results in deforming the substrates improving the transportation of the softened material. A plunge

depth (*pd*) is defined as the additional penetration of the shoulder into the workpieces from the top surface, and it ensures proper contact between the shoulder and the workpieces. It also benefits in achieving the sufficient amount of frictional heat required to deform the materials. Dissimilar materials comprising AZ31B and DP600 steel, both of 1 mm thickness, were combined for the investigation. Tables 1, 2, and 3 list the chemical composition of AZ31B, DP600, and values of ultimate tensile strength and hardness of the two substrates, respectively. Welds were fabricated by the FSW process in lap configuration, positioning the AZ31B as the advancing side (AS) above DP600 sheets in the retreating side (RS) (Fig. 1), with 30 mm being the overlapping width. A non-consumable tungsten carbide tool was used during the experiments. Fig. 2 and Fig. 3 depict the tool dimension and the location of thermocouples, respectively. Data acquisition (DAQ: National Instruments (NI) 9214) card with LABVIEW software was used to collect temperature readings. Initially, several trial experiments were conducted to obtain a suitable α and *pd* for the said combination, and the final parametric combinations have been listed in Table 4. Welds were fabricated using a dedicated computer numerically controlled (CNC) FSW machine (ETA Technology, WS004). Two weld joints were fabricated for each parametric combination of tool rotational speed and welding speed.

Table 1 AZ31 – Chemical composition (in wt. %)

List of elements	Al	Zn	Mn	Mg
Composition (in wt. %)	2.97	0.82	0.44	Bal.

Table 2 DP600 – Chemical composition (in wt. %)

List of elements	C	Mn	Si	P	Al	Fe
Composition (in wt. %)	0.09	0.86	0.34	0.01	0.03	Bal.

Table 3 UTS and hardness of substrates

Properties	**AZ31B**	**DP600**
Ultimate tensile strength (MPa)	245	656
Hardness (HV)	56	203

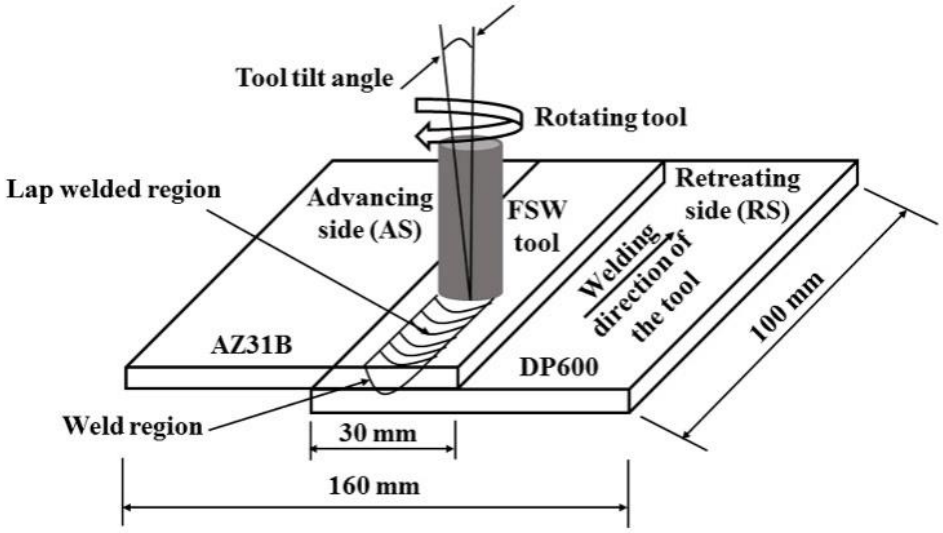

Fig. 1. Schematic illustration of FSW lap joints

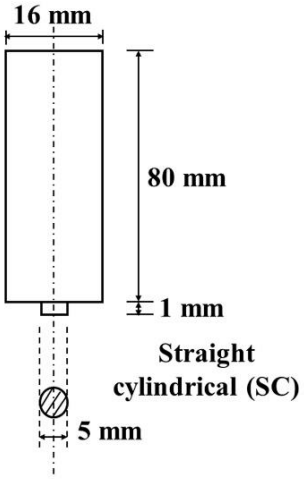

Fig. 2. Dimensions of FSW tool

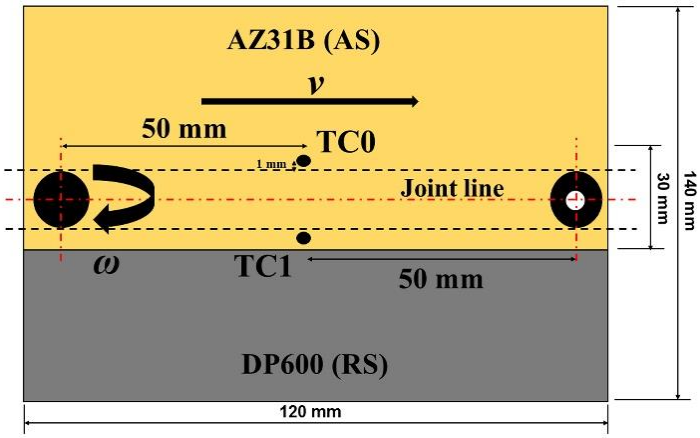

Fig. 3. Thermocouple location

Table 4 Selected FSW process parameters

Tool rotational speed (ω) (rpm)	welding speed (v) (mm/minute)	Tilt angle (α) (^{o})	Plunge depth (pd) (mm)
800	50	2	0.2
	100		
	150		
1600	50		
	100		
	150		

2.2 Characterizations of mechanical properties

Tensile tests in lap-shear configuration have been performed using a universal tensile testing machine (ZwickRoell, Kappa 100SS) by applying a 1 mm/minute crosshead speed. Dimensions of the lap-shear tensile specimen is shown in Fig. 4. The test length was

maintained as 60 mm during the test. Two samples were tested for each parametric combination.

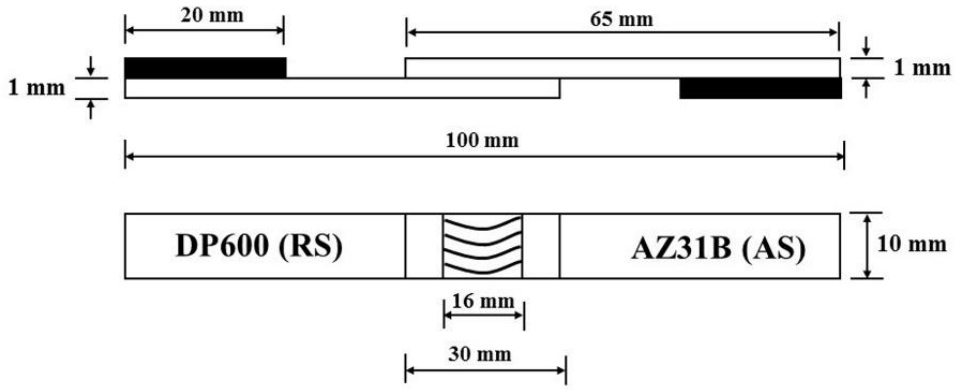

Fig. 4. Dimension of tensile shear testing sample

2.3 Microstructural characterizations

Different microstructural observations and joint interface were drawn using an inverted metallurgical OM (Leica, DMi8) and a high-resolution SEM (Zeiss, EVO18). To perform the quantitative point analysis at the stir zone (SZ), an energy dispersive spectroscopy (EDS) apparatus was utilized. The average grain size (d) was calculated by the line intersection method. The samples were mounted using poly-fast conductive powder with the help of a hot mounting press (Struers, Cito-press 15) followed by polishing. Post the mechanical polishing; the samples were etched with acetic acid (10 mL), distilled water (10 mL), ethanol (70 mL), and picric acid (4.2 gm), and nital solution, with etching time being 4 seconds for AZ31B and 30 seconds for DP600, respectively. XRD analysis of fractured surfaces was performed with the help of an XRD machine (Panalytical, Empyrean) to identify the different IMCs formed during welding.

3 Results and discussion

3.1 Spindle torque and weld surface appearance

The spindle torque and surface appearance of the joints fabricated with different parametric combinations are shown in Fig. 5. The obtained average spindle torque values during the welding stage are mentioned in Table 5. The average torque increased from ~ 5.5 Nm to ~ 6.8 Nm with the increase of v from 50 to 150 mm/minute at a ω of 800 rpm. The rise in the average torque was due to the less interaction time between the tool and the substrates. This reduction in interaction time decreased the frictional heat and led to less softening of the material. This resulted in a good surface appearance and did not have any irregularities on the surface (Fig. 5(a), (b), and (c)).

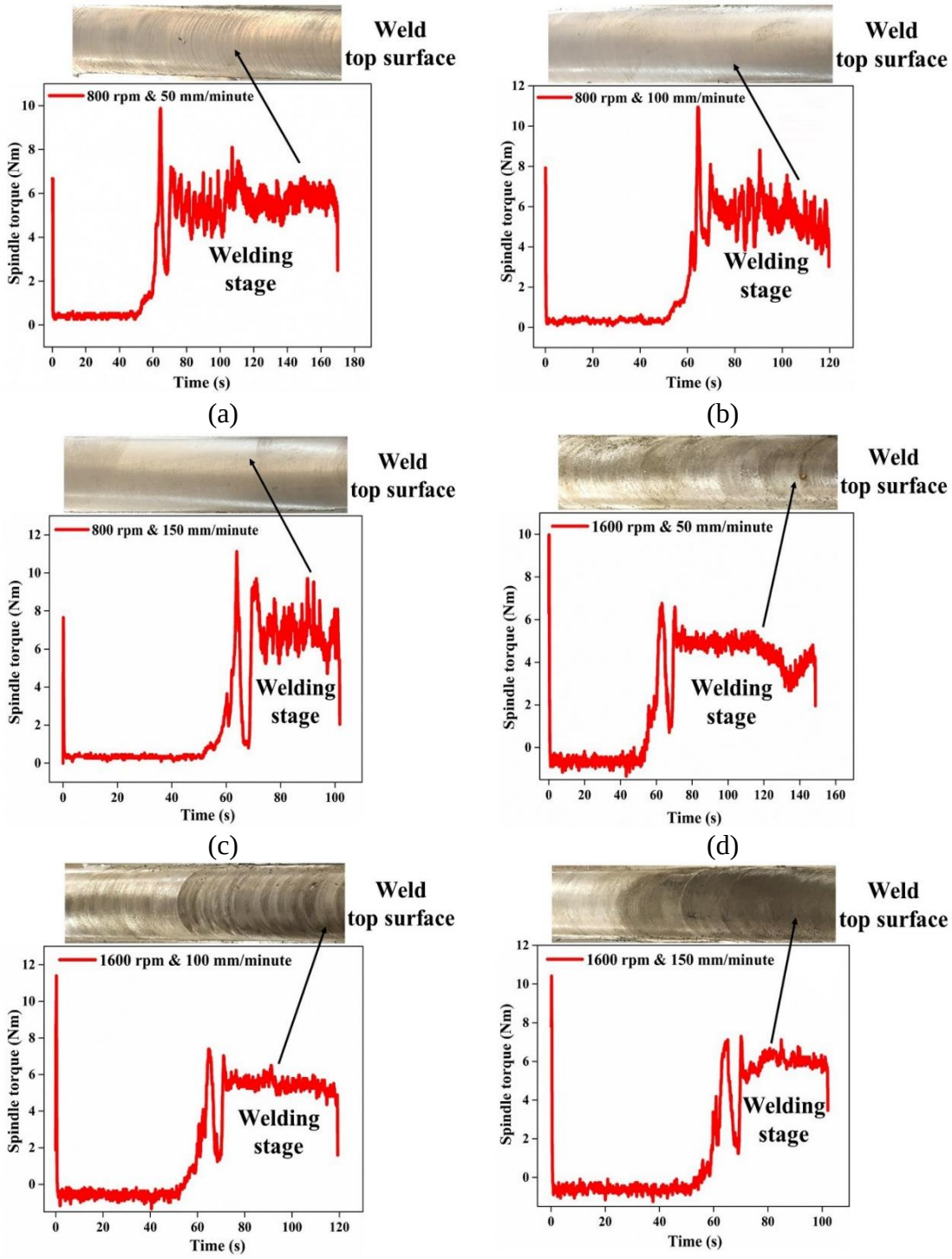

Fig. 5. Variation of spindle torque for (a), (b), and (c) for 800 rpm and v = 50, 100, and 150 mm/minute, respectively and (d), (e), and (d) for 1600 rpm and v = 50, 100, and 150 mm/minute, respectively

A fine mark of tool rotation was observed for ω of 800 rpm and v of 50 mm/minute, and the patterns were not visible for the welds fabricated with v of 100 mm/minute and 150 mm/minute. At a ω of 1600 rpm (Fig. 5(d), (e), and (f)), irrespective of the v, weld seam had rough and thin marks of the tool rotation, which was due to the higher amount of frictional heat. With high heat availability, the flowability of substrates was more which dragged the

softened Mg along with the tool shoulder. Therefore the surface was irregular with tool marks. At a *v* of 50 mm/minute, the average spindle torque during the welding stage was ~ 5.5 Nm for 800 rpm, which reduced to ~ 4.5 Nm as the ω increased to 1600 rpm. However, there was a rise in the spindle torque with the increase in *v* due to the reduction in heat input resulting in minimal material flow. During the welding stage, the average spindle torque was ~ 4.5 Nm for *v* of 50 mm/minute at ω of 1600 rpm, which augmented to ~ 5.9 Nm as the *v* increased to 150 mm/minute.

Table 5 Average spindle torque for different values of ω and *v*

Process parameters		Average spindle torque during welding stage (Nm)
Tool rotational speed (ω) (rpm)	Welding speed (*v*) (mm/minute)	
800	50	~ 5.5
	100	~ 5.6
	150	~ 6.8
1600	50	~ 4.5
	100	~ 5.4
	150	~ 5.9

3.2 Joint interface

Fig. 6 depicts the SEM images of the cross-sectional zone of weld-joints. The variation in the average height of the sawtooth profile and layered steel fragments for the present welding conditions is mentioned in Table 6. It is evident that micromechanical interlocking between the Mg/Fe lap joints has occurred when the rotating tool's pin rubs against the steel surface; the steel entity is displaced from the surface into the Mg substrate resulting in a sawtooth profile, as shown in Fig. 6. As the tool moved in the transverse direction along the joint line, an unbroken sawtooth profile is formed, which has a locking effect. For a lower value of ω, sawtooth profiles were uniform, as shown in Fig. 6(a). With an increase in ω to 1600 rpm, hardened steel fragments penetrate the soft Mg matrix dragged by the rotating tool, as shown in Fig. 6(b). The measured average height of the sawtooth profile was found to be ~ 65 µm at a ω of 800 rpm and *v* from 50 mm/minute. At a lower *v* of 50 mm/minute, the average sawtooth height was ~ 65 µm and intact. With ω increasing from 800 rpm to 1600 rpm, the sawtooth structure was transferred and relocated in a layered manner in the Mg matrix. At a higher ω of 1600 rpm, the tool had a shearing effect and caused fragmentation of the steel chips. The average height of the layered fragments increased with an increase in *v* at 1600 rpm. At ω of 1600 rpm and *v* of 50 mm/minute, the average height of the layer was higher than welding combinations, as mentioned in Table 6.

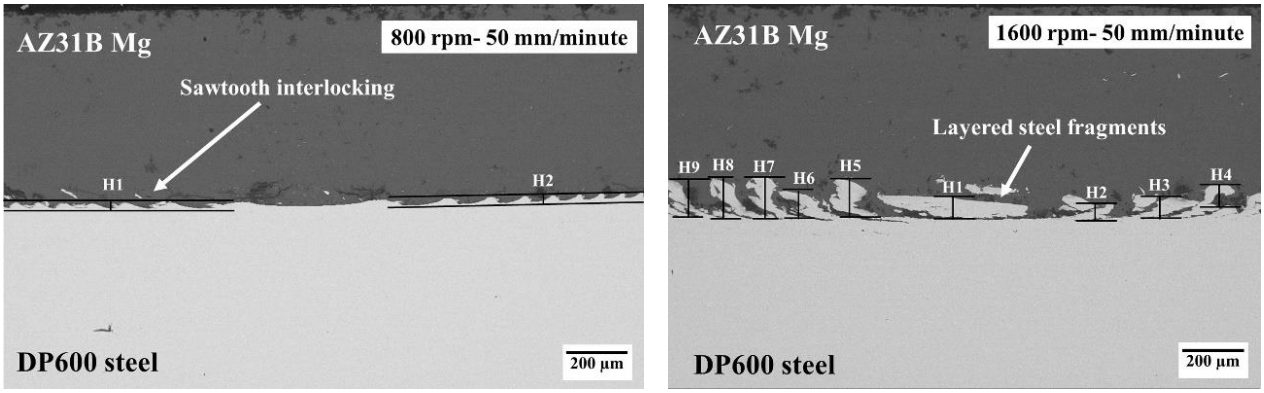

(a) (b)

Fig. 6. Interface of the weld joints for (a) ω of 800 rpm and v = 50 mm/minute and (b) ω of 1600 rpm and v = 50 mm/minute, respectively

Table 6 Average height of the sawtooth and layered steel fragments for different values of ω and v

Process parameters		The average height of the sawtooth and layered steel fragments (µm)
Tool rotational speed (ω) (rpm)	Welding speed (v) (mm/minute)	
800	50	~ 65
	100	~ 80
	150	~ 65
1600	50	~ 150
	100	~ 125
	150	~ 115

3.3 Temperature variation

The influence of v on temperature variation 1 mm away from the weld region at a ω of 800 rpm is shown in Fig. 7. With the rise in v from 50 mm/minute to 150 mm/minute, the welding temperature decreased from ~ 428 °C to ~ 334 °C, which was ~ 0.65 to 0.50 of melting temperature of AZ31B. Similarly, as shown in Fig. 8, for a ω of 1600 rpm, the welding temperature decreased from ~ 533 °C to ~ 358 °C, which was ~ 0.80 to 0.55 of the melting temperature of AZ31B Mg alloy. This temperature drop with the increase in v was because of the reduced time of contact between tool and workpiece. The influence of ω on the temperature distribution at a constant v of 50 mm/minute is shown in Fig. 7 and Fig. 8, respectively. It was observed that with the rise in ω from 800 rpm to 1600 rpm at a v of 50 mm/minute, the welding temperature raised from ~ 428 °C to ~ 533 °C, which was ~ 0.70 to 0.85 of the melting temperature of AZ31B base Mg alloy. This temperature rise was because of the higher friction between tool and substrate.

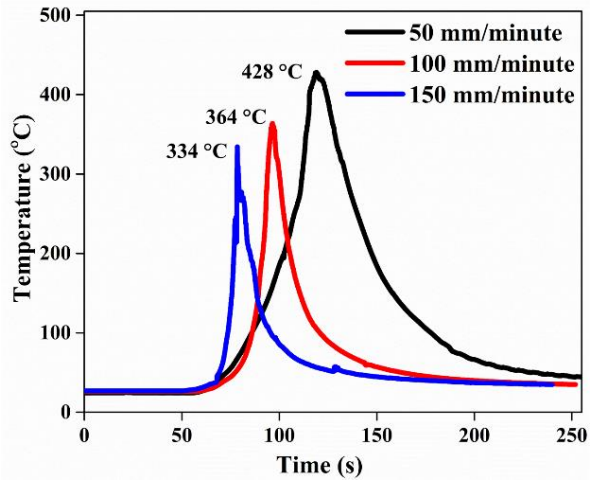

Fig. 7. Temperature-time profile for ω of 800 rpm with varying v

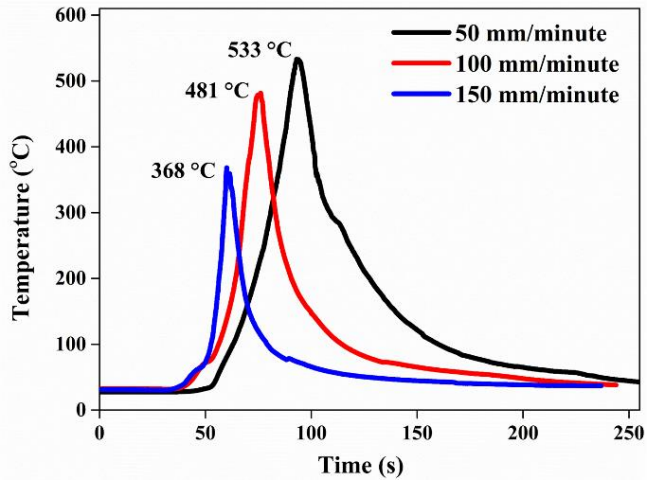

Fig. 8. Temperature-time profile for ω of 1600 rpm with varying v

3.4 Microstructural variation and joint interface characterization

Figs. 9(a) and (b) depict the optical microscopy images of the base DP600 steel and AZ31B, respectively. The DP600 steel, as shown in Fig. 9(a), exhibits phases of ferrite and martensite. Similarly, AZ31B, shown in Fig. 9(b), indicates a microstructure composed of both fine and coarser grains. The average grain size of AZ31B was found to be 28.11 µm. The overview of the cross-section of the joint fabricated with ω of 800 rpm and v of 50 mm/minute is shown in Fig. 10(a). Three distinct zones are observed, namely, (i) SZ, residing along the centreline, (ii) thermo-mechanically affected zone (TMAZ), adjacent to either side of SZ, and (iii) heat-affected zone (HAZ) adjacent to the previous zone. Optical micrographs of the different regions as indicated "(A) – (F)" in Fig. 10(b) are shown in Fig. 10(c) to (i), respectively.

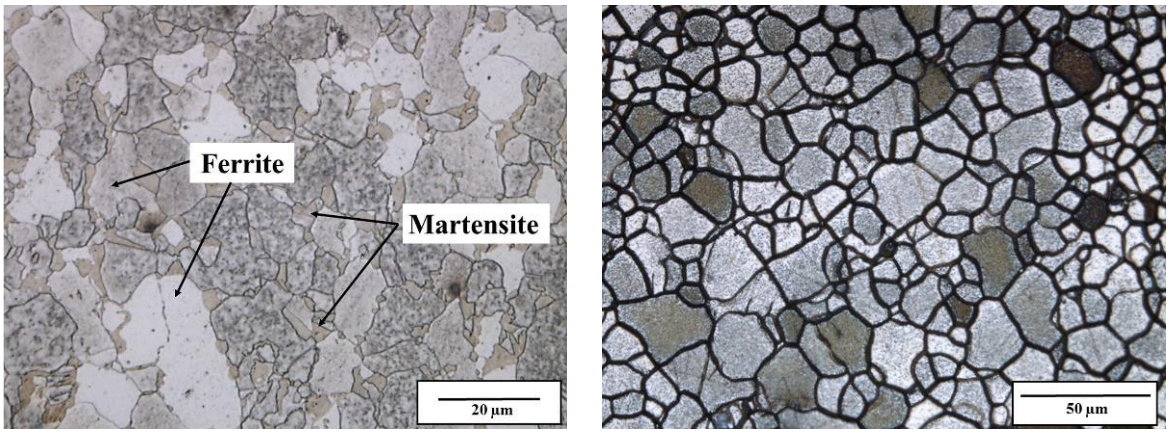

(a) (b)

Fig. 9. The microstructure of the base materials: (a) DP600 steel and (b) AZ31B magnesium alloy

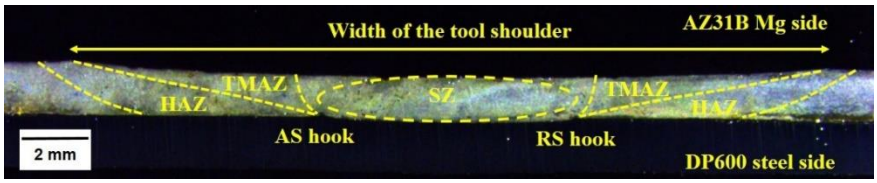

(a)

A = Upper stir zone (SZ)
B = Lower stir zone (SZ) and joint interface
C, D = Thermo-mechanically affected zone (TMAZ)
E, F = Heat affected zone (HAZ)

(b)

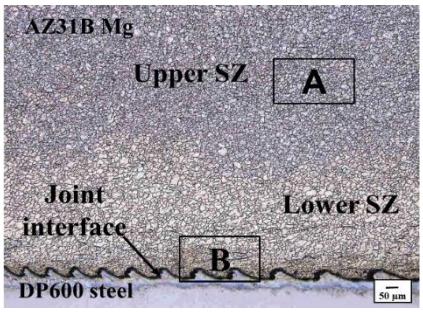

(c)

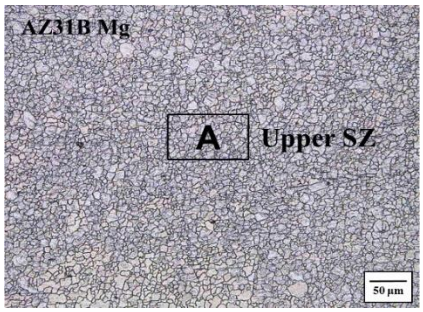

(d)

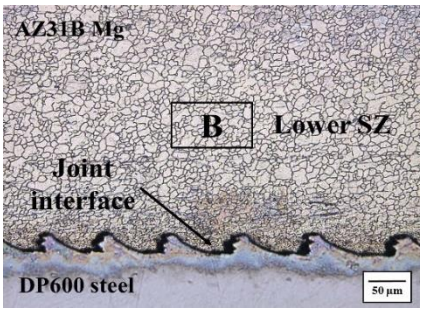

(e)

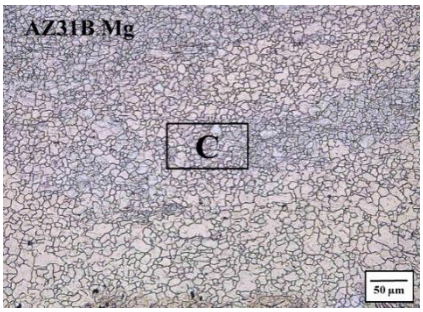

(f)

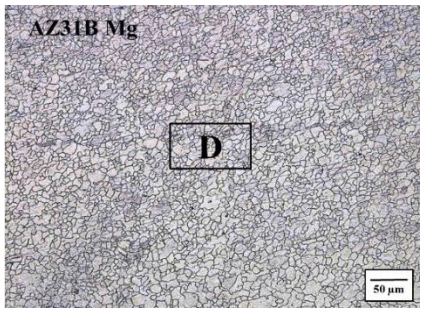

(g)

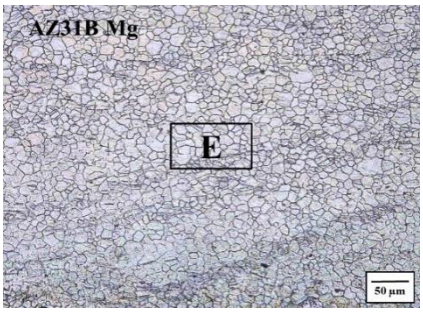

(h)

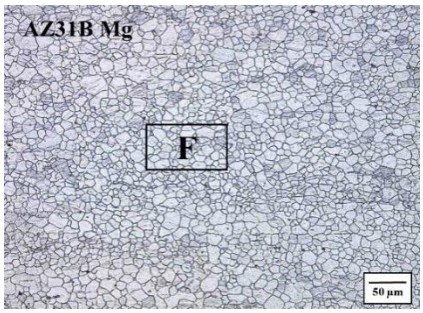

(i)

Fig. 10. Optical microscopy images showing the three distinct zones obtained for ω of 800 rpm and v of 50 mm/minute (a) overview of the cross-section (b) micro image, (c) SZ and weld interface, (d) upper SZ, (e) lower SZ and joint interface, (f), (g) TMAZ, and (h), (i) HAZ

1

Fig. 10(c) depicts the weld interface of AZ31B to DP600 and the microstructural variation at the interface, i.e., at the upper and lower part of SZ of AZ31B. Further, Fig. 10(d) and (e) depict the microstructural variations in SZ's upper and lower portions. During FSW, AZ31B undergoes significant changes in the microstructure due to the hot working caused by the rotating tool [18]. High frictional heat and severe plastic deformation steered to complete dynamic recrystallization (DRX) in SZ, which resulted in more refined grains (Fig. 10(c)). The grain sizes of SZ tend to decrease towards the top of the weld zone. This could be because of the accumulation of the material beneath the shoulder resulting in higher frictional heat. Due to this, the upper part of the SZ, as shown in Fig. 10(d), had smaller grain sizes than lower parts of the weld in SZ, as shown in Fig. 10(e). The microstructure variations in TMAZ for AS and RS are represented in Fig. 10(f) and (g), respectively. The TMAZ, which is nearer to the SZ, shows mixed zones of bulky grains and refined grains, as shown in Fig. 10(f) and (g), respectively. This indicates that the TMAZ was affected by heat and mechanical stress. The HAZ microstructure variations with respect to AS and RS are represented in Fig. 10(h) and (i), respectively. The size of the microstructure in HAZ was similar to AZ31B, with no significant growth in the grains due to this zone's lower temperature.

The OM images showing the variation of grain sizes at the SZ for different parametric combinations are shown in Fig. 11. The SZ microstructure at v of 50, 100, and 150 mm/minute with a ω of 800 rpm are represented in Fig. 11(a) - (c). Similarly, the variation of microstructure at a ω of 1600 rpm with these values of v are displayed in Fig. 11(d) – (f). The average grain size measured was 7.05 μm to 13.85 μm with ω in the range of 800 rpm to 1600 rpm, respectively indicating the occurrence of higher grain growth at higher ω compared to lower ω of 800 rpm. It could also be seen that in the present experiments, the smallest grains of 4.82 μm average size was measured for the sample welded with ω of 800 rpm and v of 150 mm/minute, respectively.

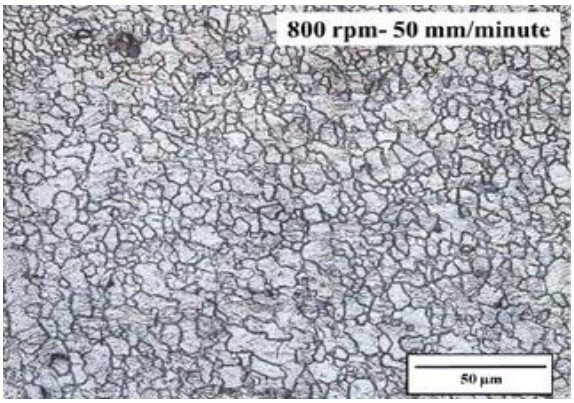

d = 7.05 µm
(a)

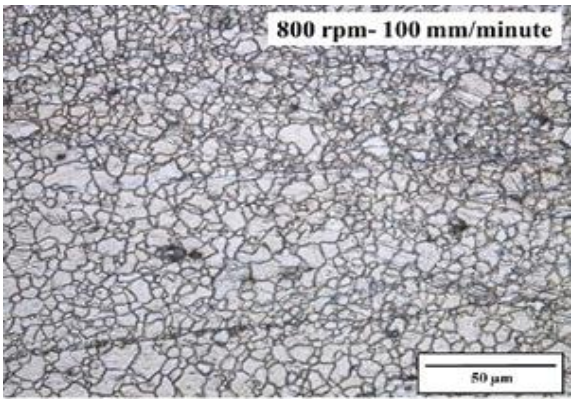

d = 5.97 µm
(b)

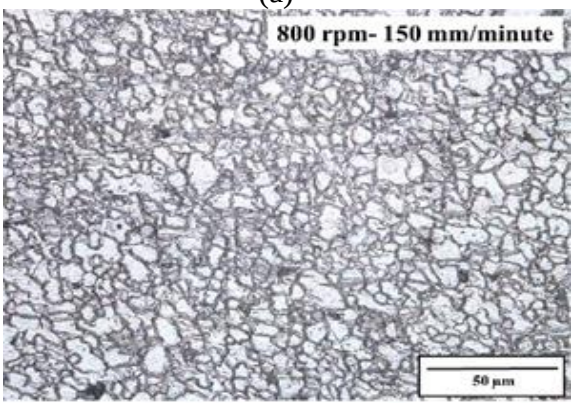

d = 4.82 µm
(c)

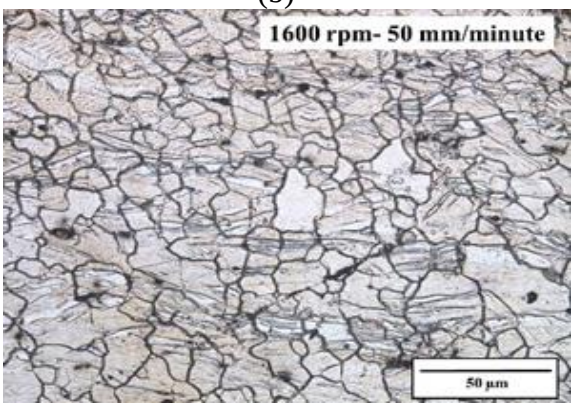

d = 13.85 µm
(d)

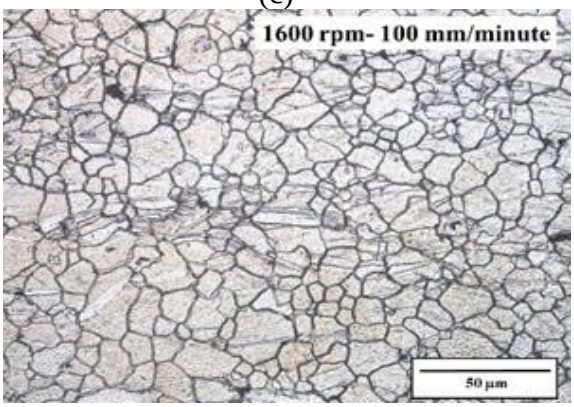

d = 12.67 µm
(e)

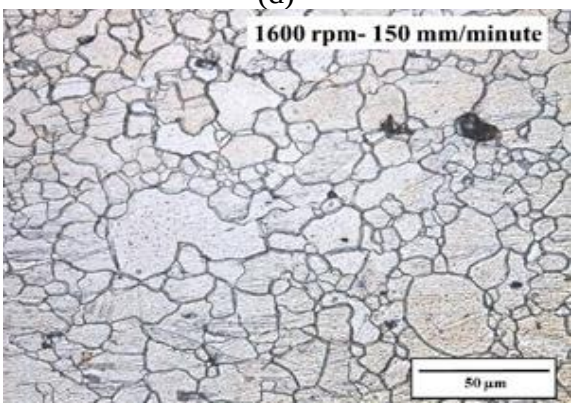

d = 11.34 µm
(f)

Fig. 11. Optical microscopy images showing variations of average grain size (d) in SZ for varying v; (a), (b) and (c) for ω of 800 rpm and (d), (e) and (f) for ω of 1600 rpm

EDS point analysis has been conducted to study further the inter-diffusion phenomenon of Mg and Fe elements. A total of 5 points were taken along the thickness direction, among them two from AZ31B side, two from DP600 side, and one at weld interface as shown in Fig. 12. The obtained chemical compositions for varying welding conditions are mentioned in the respective figures. When the analysis was performed on the Mg side, the Fe component is absent. However, the Mg element was detected at the Fe side close to the interface of the

joint. It has been observed from Fig. 12, for all the weld joints, the Fe atoms diffused into the Mg side at the weld interface.

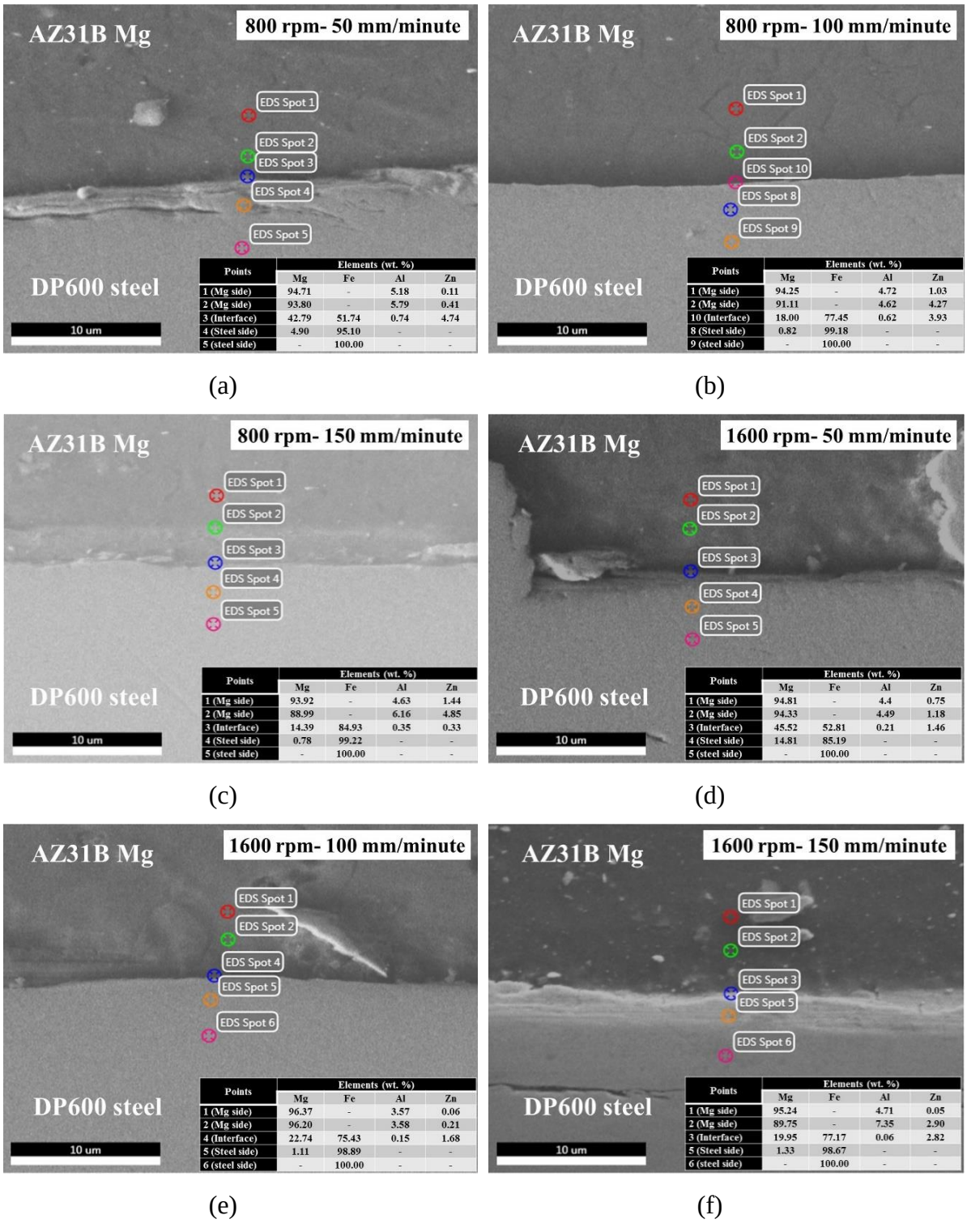

Fig. 12. EDS quantitative point elemental analysis at the interface of the joint for different ω and v

Furthermore, with the rise in v from 50 mm/minute to 150 mm/minute at ω of 800 rpm, the Mg concentration has decreased, as shown in Fig. 12(a) - (c). This could be due to the lower value of v, which caused severe plastic deformation resulting in better mixing of the material at the joint interface and higher Mg concentration. Similar observations are also found for ω of 1600 rpm, as shown in Fig. 12(d) - (f). It has also been observed that the concentration of Al is higher at lower values of ω, i.e., 800 rpm, as compared to higher ω, i.e., 1600 rpm. As Al and Zn are two major alloying elements in AZ31B Mg alloy, both Al/Fe and Mg/Zn IMCs could be possible and further to identify the IMCs at the interface of the joints, XRD analysis was performed.

3.5 Lap shear test and morphology of fracture surface

Fig. 13 shows the result of the lap shear tests at different ω and v. Hook heights, and the weld efficiency of the samples welded to varying values of process parameters are tabulated in Table 7. The failure load of the weld joint was found to be lower than AZ31B base material. For joint fabricated with ω of 800 rpm and v of 50 mm/minute, failure load was 1871.6 N, and joint efficiency was 76.4%, and this was the maximum achieved failure load among other conditions. The uniform and close contact between Mg and steel attributed to this maximum failure load. With the rise in v from 50 to 150 mm/minute, the grain size was small because of reduced hold time, permitting just recrystallization; no grain growth was observed. But for the ω of 1600 rpm, failure load of 1618.1 N was attained at higher values of v of 150 mm/minute. In the case of high ω, the failure load increased with v. For higher ω of 1600 rpm, higher heat generated at lower v of 50 mm/minute caused softening of the materials at the joint interface and grain coarsening. Due to the softening effect at the joint interface, the softer steel was dragged towards the upper Mg alloy by the FSW tool. This reduced the effective Mg sheet thickness resulting in a poor locking effect, and was responsible for a reduced failure load of 1107.3 N. As v was increased, the height was suppressed, and the steel fragmented layers were uniform, resulting in better joint strength.

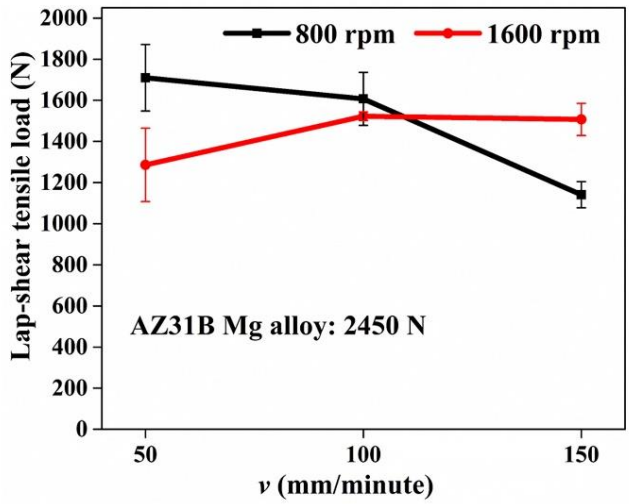

Fig. 13. Lap shear load variations with respect to ω and v

Table 7 Heat index, hook height, maximum strength, and joint efficiency with respect to ω and v

Process parameters		Heat Index (HI) $\frac{\omega^2}{v \times 10^4}$	Hook height (μm)	Maximum lap shear failure load (N)	Weld efficiency (%)
Tool rotational speed (ω) (rpm)	Welding speed (v) (mm/minute)				
800	50	1.28	49	1871.6	76.4
	100	0.64	78	1735.7	70.8
	150	0.42	92	1326.4	54.1
1600	50	5.12	390	1464.9	59.8
	100	2.56	272	1543.4	63.0
	150	1.70	190	1618.1	66.0

The fracture position of the joints after the lap shear test is shown in Fig. 14. All the tensile samples failed from the joint hook at the RS and along the SZ boundary extended towards the top surface of the Mg alloy plate. Hook in lap joints caused the local thinning of the effective sheet thickness, and the microstructure along the fracture pathway was responsible for reducing joint strength. Further, the effect of ω and v on hook phenomenon are discussed.

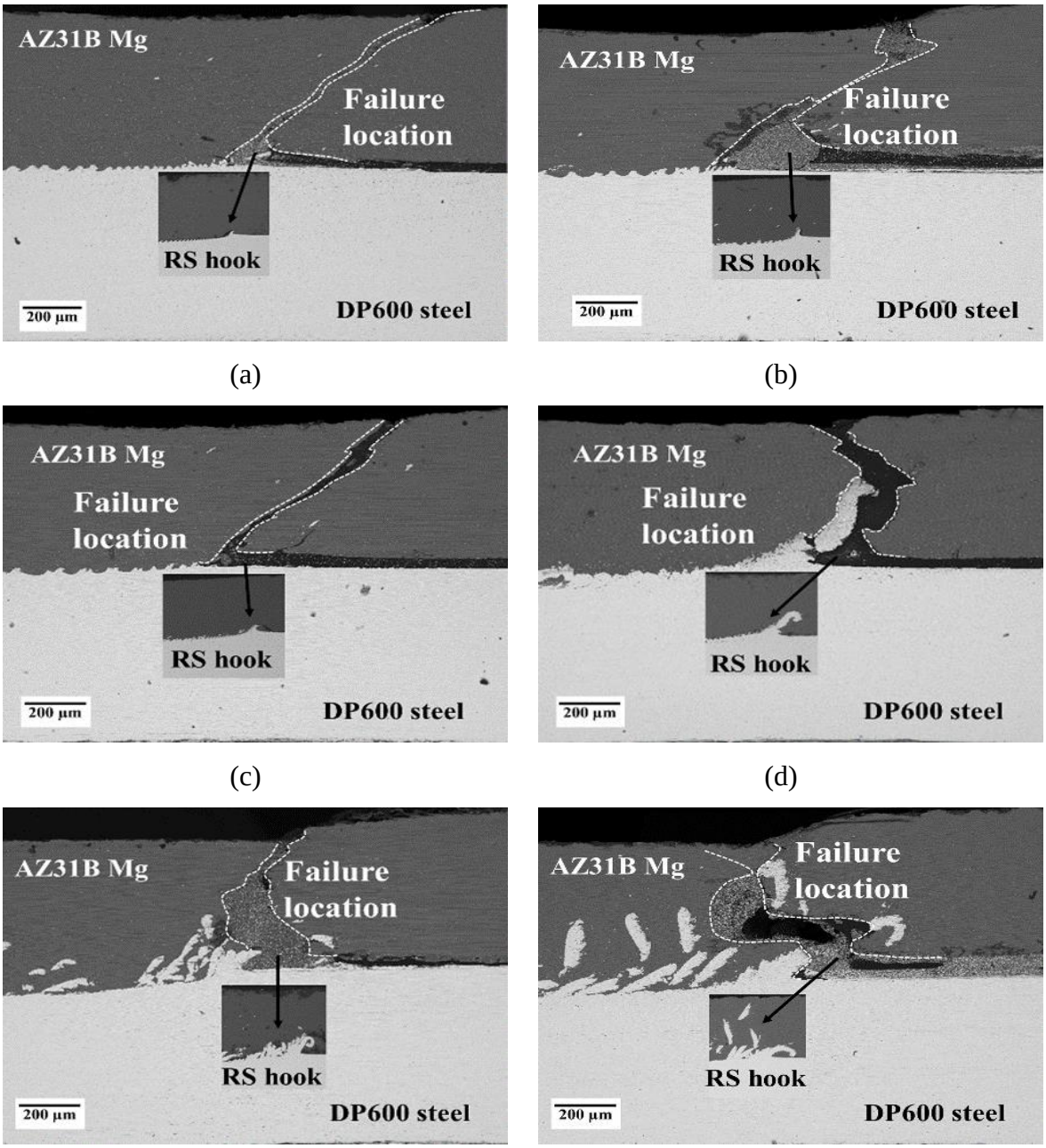

Fig. 14. Fracture position for different welding conditions; (a), (b), and (c) for 800 rpm and v = 50, 100, and 150 mm/minute, respectively, (d), (e), and (d) for 1600 rpm and v = 50, 100, and 150 mm/minute, respectively

Fig. 15 represents the SEM images of the hook. To understand the effect of heat input on hook characteristics, a pseudo heat index (HI) parameter, which is defined as HI = $\omega^2/(v \times 10^4)$ [17] has been considered by using ω and v. The values of HI for different values of ω and v are mentioned in Table 8. Further, the relation between HI and hook height is depicted in Fig. 16. It has been observed that with the rise in v from 50 to 150 mm/minute at a ω of 800 rpm, HI decreased from 1.28 to 0.42, and the hook height increased from 49

μm to 92 μm. However, with the rise in v from 50 to 150 mm/minute at a ω of 1600 rpm, both HI (5.12 to 1.70) and the hook height (390 μm to 190 μm) decreased. At lower ω of 800 rpm, the HI values for different values of v are smaller, as shown in Fig. 16. Due to lower HI, the interface is relatively cold compared to that at a ω of 1600 rpm, and the material transport is primarily due to the effect of dragging. With the change in v from 50 to 150 mm/minute, the faster movement of the tool shoulder and pin pulled more steel towards the Mg matrix resulting in a considerably larger hook size. At a ω of 1600 rpm, the HI values are significantly higher, as depicted in Fig. 16. Due to higher HI, the interface is relatively hot, resulting in more significant softening and more metal plasticization. This contributed to a more considerable interface lifting of steel substrate by tool shoulder and pin towards Mg matrix, resulting in larger hook size. This affects the effective thickness of the Mg sheet, and as a consequence, failure load has decreased. But, with the increase in v from 50 up to 150 mm/minute at a ω of 1600 rpm, the HI decreased. This condition thereby reduces the vertical material flow phenomenon induced by the tool, resulting in reduced hook size.

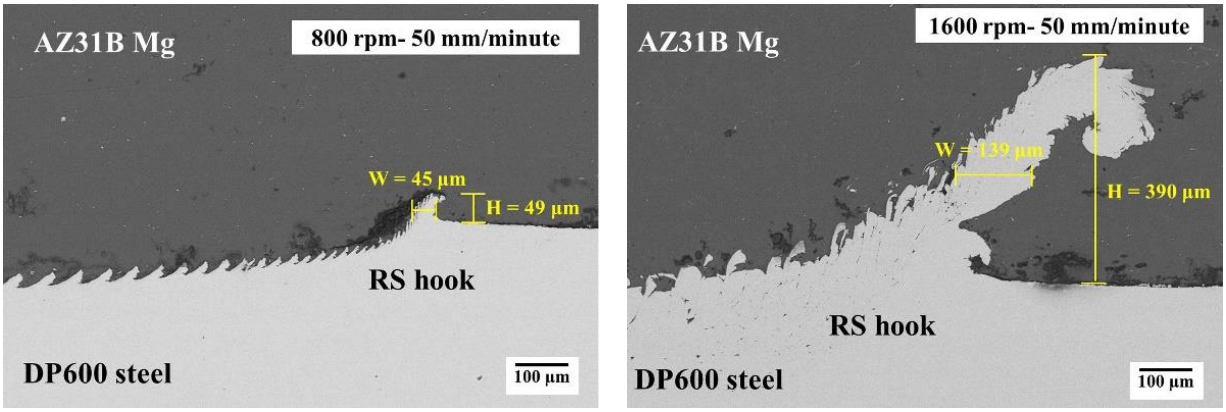

(a) (b)

Fig. 15. Hook height for(a) ω of 800 rpm and v = 50 mm/minute and (b) ω of 1600 rpm and v = 50 mm/minute, respectively

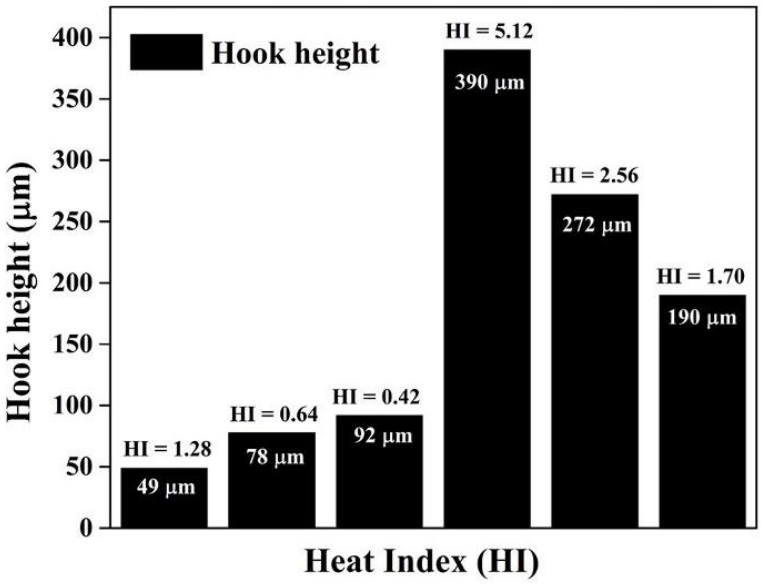

Fig. 16. Relationship between HI and hook height for the different values of ω and v

The SEM images of the fractured surface of the AZ31B base alloy and that of the welded samples are shown in Fig. 17 and Fig. 18, respectively. Very fine dimples and tearing ridges were found in base Mg alloy, indicating ductile fracture characteristics. The size of the dimples varied between 8 to 15 μm for base Mg alloy. However, in the case of welds, it was observed that the fracture surfaces were comprised of dimples of both small and large sizes, tearing ridges, and cleavage facets indicating both ductile and brittle modes of fracture characteristics. The dimple size at ω of 800 rpm was found in between 10 to 15 μm. Similarly, for the ω of 1600 rpm, the dimple's average size increased between 19 to 34 μm. The variation of the size of the dimples at ω of 800 rpm was lower as compared to ω of 1600 rpm, which could be due to the formation of finer grains, which significantly enhanced the resistance to tensile deformation during testing.

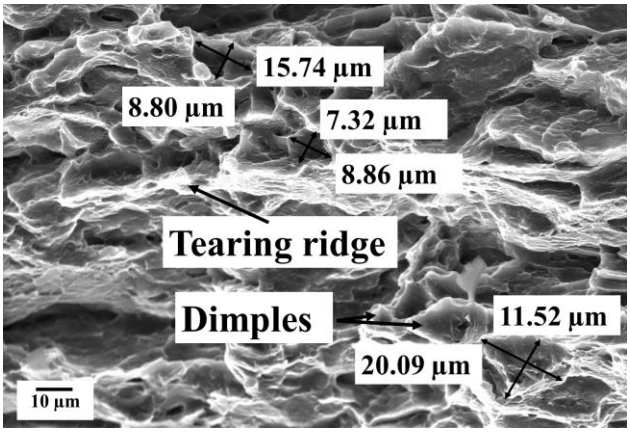

Fig. 17. Fracture surface morphology of AZ31B base Mg alloy

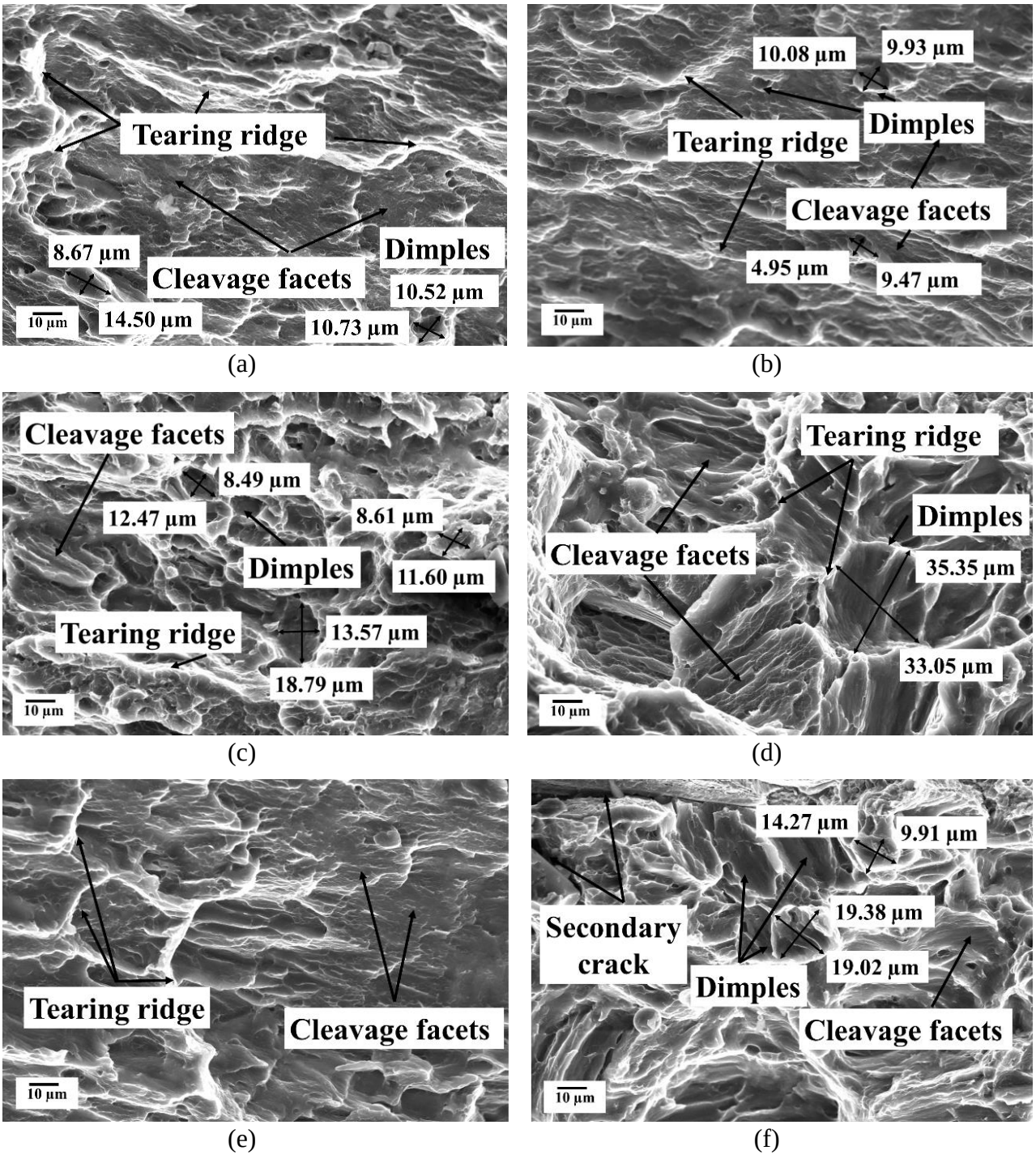

Fig. 18. Fracture surface morphology of different welds; (a), (b), and (c) for ω of 800 rpm and v of 50, 100, and 150 mm/minute, respectively, (d), (e), and (d) for ω of 1600 rpm and v of 50, 100, and 150 mm/minute, respectively

3.6 Fracture surface phase analysis through XRD

The XRD phase analyses of the fracture surfaces of the welded samples were performed on the AZ31B side to identify the presence of different IMCs. The XRD plots for the base materials (AZ31B Mg alloy and DP600 steel) are represented in Fig. 19. The significant peaks of the base AZ31B Mg alloy were observed at 34.399° and 36.620°, corresponding to (002) and (101) planes of Mg, as shown in Fig. 19(a). Similarly, for base DP600 steel, the

major Fe peaks were found at 44.674° and 82.335°, corresponding to (110) and (211) planes of Fe, respectively. This has been shown in Fig. 19(b). The XRD spectra of the fractured AZ31B/DP600 weld joints for different values of ω of 800 and 1600 rpm have been shown in Fig. 20(a) and (b), respectively, at the Mg side. Although the peaks belonging to phases of Mg and Fe were observed, the formation of any IMC has not been seen. This could be due to the immiscibility characteristics of both materials. The peaks corresponding to the intermetallic of Al/Fe and Mg/Zn were observed through the XRD analyses. Phases of Al/Fe, i.e., AlFe, were detected at 44.370° and 81.506°, corresponding to (110) and (211) planes, respectively. This could be due to the high content of Al in the AZ31B Mg alloy, which makes it possible to form AlFe IMC at the Mg/steel interface. Similarly, phases of Mg/Zn, i.e., $Mg_{0.97}Zn_{0.03}$ was created due to diffusion of Zn atom in the crystal structure of Mg at 32.391°, 36.854°, and 70.525° corresponding to (100), (101), and (211) planes, respectively.

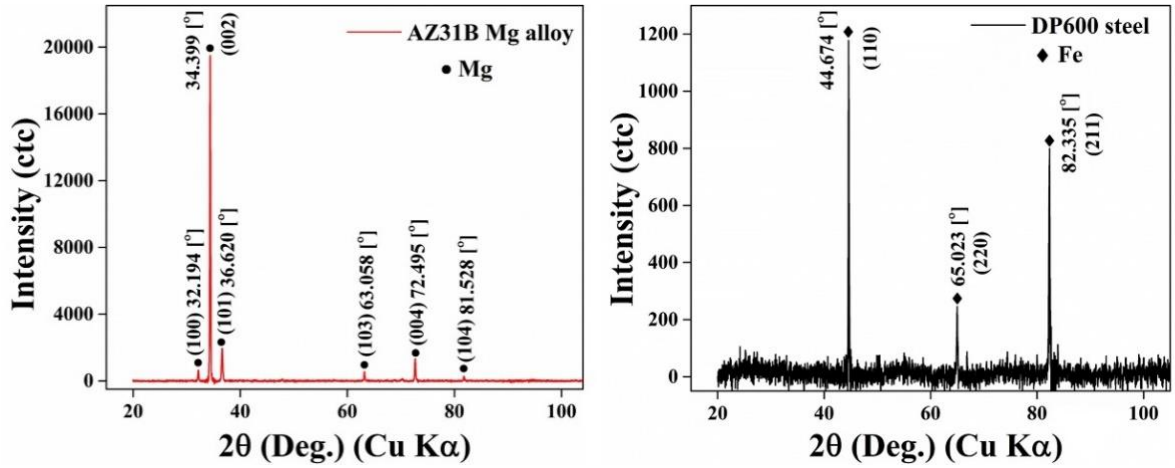

(a) (b)

Fig. 19. XRD analyses for base materials: (a) AZ31B Mg alloy and (b) DP600 steel

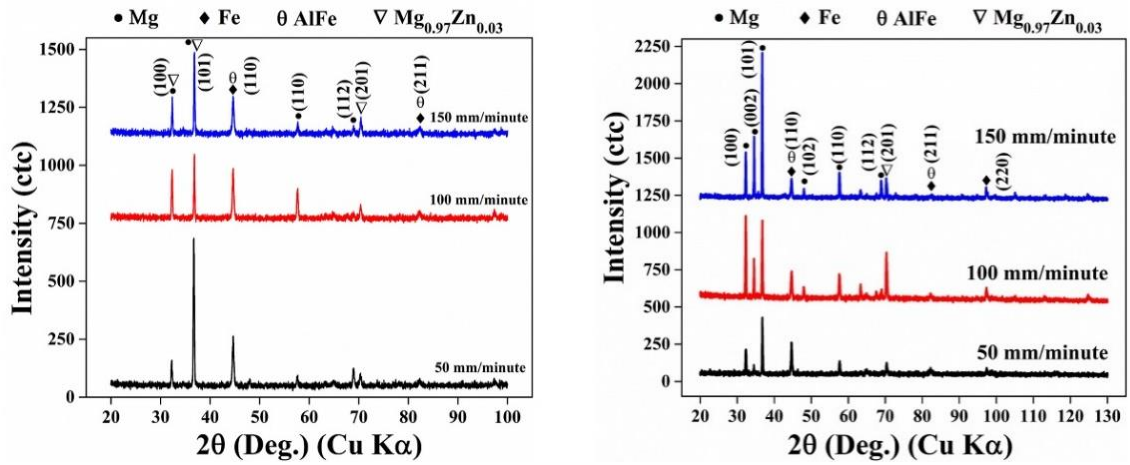

(a) (b)

Fig. 20. XRD analysis on AZ31B Mg side; (a) ω of 800 rpm and (b) ω of 1600 rpm

Conclusions

The present study demonstrates the implementation of the FSW technique to weld Mg and steel in lap joint configuration. The following conclusions can be made based on the present study.

1. Under different process parameter combinations, the measured average height of the sawtooth profile was found to be ~ 65 μm for ω of 800 rpm and v from 50 mm/minute. The maximum average height of ~ 150 μm was measured for ω of 1600 rpm and v from 50 mm/minute for the present process parameters.
2. A maximum temperature of ~ 533 °C was observed for the weld fabricated with ω of 1600 rpm and v of 50 mm/minute. The minimum temperature of ~ 334 °C was observed for the joint developed with ω of 800 rpm and v of 150 mm/minute. The variation in the temperature and duration was because of the friction and traversing between tool and substrate.
3. The minimum average grain size of 4.82 μm was measured for the sample welded with ω of 800 rpm and v of 150 mm/minute. Similarly, the maximum average grain size of 13.85 μm was measured for the sample welded with ω of 1600 rpm and v of 50 mm/minute, respectively.
4. Weld fabricated with ω of 800 rpm and v of 50 mm/minute has the higher failure load of 1871.6 N for the present experimental condition. The efficiency of the joint varies between 54% to 76% for different process parameters. The tensile failure of all the samples failed near the hook location. From the fracture surface morphology characteristics, it has been concluded that the fracture surfaces were composed of various sizes of dimples, tearing ridges, and cleavage facets, indicating both ductile and brittle mode of fracture during the tensile failure.
5. Among the studied weld process parameters, depending upon the heat generated, the minimum and maximum heights of the hook of 49 μm and 390 μm were observed for ω of 800 rpm and 1600 rpm, respectively, at a v of 50 mm/minute.
6. Mutual diffusion between Fe and Mg has been found with the presence of IMCs such as AlFe and Mg0.97Zn0.03 at the fracture surface.

Acknowledgment

Authors are thankful to the *"Materials Welding and Joining, Research and Development"* division of TATA STEEL for providing the DP600 steel sheets and *"Centre of Excellence in Advanced Manufacturing Technology"* of IIT Kharagpur for extending the characterization facilities

Funding: The authors did not receive any financial support from any organization for the submitted work.

Compliance with Ethical Standards

Conflict of interest: There are no potential conflicts of interest involved in the present study.

Human and animal rights: This article does not contain any studies with human participants or animals performed by any of the authors.

Informed consent: This article does not contain any studies with human participants or animals performed by any of the authors.

References

[1] Martinsen K, Hu SJ, Carlson BE. Joining of dissimilar materials. CIRP Ann - Manuf Technol 2015;64:679–99. doi:10.1016/j.cirp.2015.05.006.

[2] Mallick PK. Joining for lightweight vehicles. Woodhead Publishing Limited; 2010. doi:10.1533/9781845697822.2.275.

[3] Wang W, Han P, Qiao K, Li T, Wang K, Cai J. E ff ect of the rotation rate on the low-cycle fatigue behavior of friction-stir welded AZ31 magnesium alloy. Eng Fract Mech 2020;228:106925. doi:10.1016/j.engfracmech.2020.106925.

[4] Monteiro WA, Buso SJ, Silva LV da. Application of Magnesium Alloys in Transport. In: Monteiro WA, editor. New Featur. Magnes. Alloy., intechopen; 2012, p. 3938. doi:10.5772/2810.

[5] Tasan CC, Diehl M, Yan D, Bechtold M, Roters F, Schemmann L, et al. An Overview of Dual-Phase Steels: Advances in Microstructure-Oriented Processing and Micromechanically Guided Design. Annu Rev Mater Res 2015;45:391–431. doi:10.1146/annurev-matsci-070214-021103.

[6] Chen YC, Nakata K. Effect of tool geometry on microstructure and mechanical properties of friction stir lap welded magnesium alloy and steel. Mater Des 2009;30:3913–9. doi:10.1016/j.matdes.2009.03.007.

[7] Jana S, Hovanski Y, Grant GJ. Friction stir lap welding of magnesium alloy to steel: A preliminary investigation. Metall Mater Trans A Phys Metall Mater Sci 2010;41:3173–82. doi:10.1007/s11661-010-0399-8.

[8] Wayne MT, Edward DN, James CN, Michael GM, Smith PT. Friction Stir Welding.

PatentApplication No PCTrGB92 Patent Application No.9125978.8, 1991.

[9] Amini A, Asadi P, Zolghadr P. Friction stir welding applications in industry. Woodhead Publishing Limited; 2014. doi:10.1533/9780857094551.671.

[10] Kusuda Y. Honda develops robotized FSW technology to weld steel and aluminum and applied it to a mass-production vehicle. Ind Robot An Int J 2013;40:208–12. doi:10.1108/01439911311309889.

[11] Mahto RP, Bhoje R, Pal SK, Joshi HS, Das S. A study on mechanical properties in friction stir lap welding of AA 6061-T6 and AISI 304. Mater Sci Eng A 2016;652:136–44. doi:10.1016/j.msea.2015.11.064.

[12] Chen YC, Nakata K. Friction Stir Lap Welding of Magnesium Alloy and Zinc-Coated Steel. Mater Trans 2009;50:2598–603. doi:10.2320/matertrans.M2009022.

[13] Schneider C, Weinberger T, Inoue J, Koseki T, Enzinger N. Characterisation of interface of steel/magnesium FSW. Sci Technol Weld Join 2011;16:100–7. doi:10.1179/1362171810Y.0000000012.

[14] Wei Y, Li J, Xiong J, Huang F, Zhang F. Microstructures and mechanical properties of magnesium alloy and stainless steel weld-joint made by friction stir lap welding. Mater Des 2012;33:111–4. doi:10.1016/j.matdes.2011.07.016.

[15] Chen YC, Nakata K. Effect of surface states of steel on microstructure and mechanical properties of lap joints of magnesium alloy and steel by friction stir welding. Sci Technol Weld Join 2010;15:293–8. doi:10.1179/136217109X12568132624325.

[16] Vora Jaykumar, J., Badheka Vishvesh, J. Advances in Welding Technologies for Process Development. CRC Press Taylor & Francis Group; 2019.

[17] QUERIN J, SCHNEIDER J. Developing an Alternative Heat Indexing Equation for FSW. Weld J 2012;91:76–82.